INSTITUT DE FRANCE
Académie des sciences

Comptes Rendus

Chimie

Lucas Henry, Dominique Bazin, Clotilde Policar, Jean-Philippe Haymann, Michel Daudon, Vincent Frochot and Muriel Mathonnet

Characterization through scanning electron microscopy and μFourier transform infrared spectroscopy of microcalcifications present in fine needle aspiration smears

Volume 25, Special Issue S1 (2022), p. 503-515

Published online: 27 July 2022

https://doi.org/10.5802/crchim.187

Part of Special Issue: Microcrystalline pathologies: Clinical issues and nanochemistry

Guest editors: Dominique Bazin (Université Paris-Saclay, CNRS, ICP, France), Michel Daudon, Vincent Frochot, Emmanuel Letavernier and Jean-Philippe Haymann (Sorbonne Université, INSERM, AP-HP, Hôpital Tenon, France)

This article is licensed under the
Creative Commons Attribution 4.0 International License.
http://creativecommons.org/licenses/by/4.0/

Les Comptes Rendus. Chimie *sont membres du*
Centre Mersenne pour l'édition scientifique ouverte
www.centre-mersenne.org
e-ISSN : 1878-1543

Comptes Rendus
Chimie
2022, Vol. 25, Special Issue S1, p. 503-515
https://doi.org/10.5802/crchim.187

Microcrystalline pathologies: Clinical issues and nanochemistry / *Pathologies microcristallines : questions cliniques et nanochimie*

Characterization through scanning electron microscopy and μFourier transform infrared spectroscopy of microcalcifications present in fine needle aspiration smears

Caractérisation par microscopie électronique à balayage et microspectroscopie infrarouge de dépôts anormaux présents dans des ponctions thyroïdiennes

Lucas Henry [a], Dominique Bazin [*, b, c], Clotilde Policar [a], Jean-Philippe Haymann [d, e], Michel Daudon [d, e], Vincent Frochot [d, e] and Muriel Mathonnet [f]

[a] Laboratoire des BioMolécules, LBM, Département de chimie, École normale supérieure, PSL University, Sorbonne Université, CNRS, F-75005 Paris, France

[b] Laboratoire de Chimie Physique, Université Paris Saclay, 310, rue Michel Magat, 91400 Orsay, France

[c] Laboratoire de Physique des Solides, Université Paris Saclay, 91400 Orsay, France

[d] INSERM, UMRS 1155, UPMC, Hôpital Tenon, 75970 Paris, France

[e] Service d'explorations fonctionnelles, Hôpital Tenon, AP-HP, 4, rue de la Chine, 75970 Paris Cedex 20, France

[f] Service de chirurgie digestive, générale et endocrinienne, CHU Dupuytren, Limoges, France

E-mails: lucas.henry@ens.fr (L. Henry), dominique.bazin@universite-paris-saclay.fr (D. Bazin), clotilde.policar@ens.psl.eu (C. Policar), jean-philippe.haymann@tnn.aphp.fr (J.-P. Haymann), daudonmichel24@gmail.com (M. Daudon), vincent.frochot@aphp.fr (V. Frochot), muriel.mathonnet@unilim.fr (M. Mathonnet)

Abstract. In this contribution, we have characterized for the first time (to the best of our knowledge), microcalcifications present in fine needle aspiration (FNA) smears of thyroid nodules. Abnormal deposits were analysed through μFourier Transform Infrared Spectroscopy (μFTIR) and Field Emission

* Corresponding author.

Scanning Electron Microscopy (FE-SEM) in order to obtain their chemical composition as well as their morphology at the micrometer scale. Thirty-one samples coming from 13 patients were investigated comprising five cases of papillary carcinoma, two of Graves' disease, and six of adenomatous goitre. The smears were also stained for analysis of the cellular characteristics of these lesions for classifying according to the Bethesda classification. Two mineral species, amorphous and nanocrystallised apatite calcium phosphate, have been identified with very different morphologies. Moreover, FE-SEM observations at the micrometer scale underline the presence of different kinds of abnormal deposits.

Résumé. Dans cette contribution, nous avons caractérisé pour la première fois à notre connaissance, les microcalcifications présentes dans les ponctions thyroïdiennes. Les dépôts anormaux ont été analysés par micro spectroscopie infrarouge à transformée de Fourier et par microscopie électronique à balayage à émission de champ (FE-SEM) afin d'obtenir leur composition chimique ainsi que leur morphologie à l'échelle micrométrique. Trente et un échantillons provenant de 13 patients ont été étudiés, dont 5 cas de carcinome papillaire, 2 de maladie de Basedow et 6 de goitre adénomateux. Les ponctions ont également été colorées pour analyser les caractéristiques cellulaires de ces lésions afin de les classer selon la classification de Bethesda. Deux espèces minérales, le phosphate de calcium apatite amorphe et nanocristallisé, ont été identifiées avec des morphologies très différentes. De plus, les observations FE-SEM à l'échelle micrométrique soulignent la présence de différents types de dépôts anormaux.

Keywords. Thyroid, Nodule, Smears, Infrared spectroscopy, Scanning electron microscopy.

Mots-clés. Thyroïde, Nodule, Ponctions, Spectroscopie infrarouge, Microscopie électronique à balayage.

Published online: 27 July 2022

1. Introduction

The most common thyroid disease in the community is simple (diffuse) physiological goitre [1]. While the prevalence of diffuse goitre declines with age, different investigations underline an increase in frequency of thyroid nodules and thyroid antibodies with age. More precisely, epidemiologic investigations suggest that nodular thyroid disease is a common clinical problem, with a prevalence of nodules in 4%–7% of the adult population.

Thyroid nodules [2–7] as well as thyroid calcifications [8–14] are observed for different thyroid pathologies. Recently, we have conducted two physicochemical investigations on thyroid macrocalcifications for patients corresponding to Grave's disease, papillary carcinoma, benign nodules, multinodular goitre [15,16]. Two characterization techniques, namely μFourier Transform Infrared Spectroscopy (μFTIR) [17–20] and Field Emission Scanning Electron Microscopy (FE-SEM) [18–21] were used in order to assess a possible relationship between the pathology and the physicochemical characteristics of the macrocalcifications. Such approaches have been already developed for microcalcifications in organs such as the kidney showing that the morphology of the crystallites of which the agglomeration gives the macrocalcifications as well as their chemical identification are of major importance [22–25]. Such complexity calls for physicochemical techniques to characterize such deposits which may exist also at the micrometer and at the nanometer scales [26–31].

At this point, we have to recall that a careful analysis of the IR absorption spectra of thyroid tissue revealed the presence of amorphous and nanocrystallized calcium phosphate apatite, calcium oxalate monohydrate and/or dihydrate as well as triglycerides and cholesterol [15,16]. The complete set of data we have obtained on these macrocalcifications seems to indicate that there is no clear relationship between their chemical composition and the disease. Nevertheless, from a biochemical point of view, the presence of the various types of crystals is a marker of very different biological conditions, and as such, of different pathologies [22–25].

Though the presence of microcalcifications in smears has already been attested, very little information exists on their chemical composition. The aim of our work was to analyze the composition of thyroid microcalcifications from smears obtained by ultrasound-guided fine needle puncture. Such an approach is a first step to establish a possible relationship between the physico-chemistry of abnormal deposits in thyroid smears and the disease which induces their formation.

Table 1. Clinical data and chemical compounds identified in smears of thyroid biopsies for patients with sclerosing variant of papillary thyroid carcinoma stage 3 or papillary thyroid carcinoma

Samples	Sex and age	FTIR analysis	Bethesda classification	Pathology
Patient 1 Biopsy 1	M, 14	Presence of lipids without calcifications	5	Sclerosing variant of papillary thyroid carcinoma stage 3
Patient 1 Biopsy 2	M, 14	Presence of CA	5	Sclerosing variant of papillary thyroid carcinoma stage 3
Patient 1 Biopsy 3	M, 14	Presence of CA and glycoprotein	5	Sclerosing variant of papillary thyroid carcinoma stage 3
Patient 1 Biopsy 4	M, 14	Sample without apatite but note the presence of polysaccharides	5	Sclerosing variant of papillary thyroid carcinoma stage 3
Patient 2 Biopsy 1	M, 75	Some calcifications made of CA have been detected. Presence of acicular calcifications	5	Papillary thyroid carcinoma stage 3
Patient 2 Biopsy 2	M, 75	Some calcifications made of CA have been detected	5	Papillary thyroid carcinoma stage 3
Patient 3 Biopsy 1	F, 34	Some calcifications made of CA have been detected	1	Papillary thyroid carcinoma stage 1
Patient 3 Biopsy 2	F, 34	Some spherical calcifications made of CA have been detected	1	Papillary thyroid carcinoma stage 1
Patient 4 Biopsy 1	F, 51	The deposit was too thick	1	Papillary thyroid carcinoma stage 2
Patient 4 Biopsy 2	F, 51	Sample without apatite but note the presence of polysaccharides	1	Papillary thyroid carcinoma stage 2
Patient 5 Biopsy 1	M, 42	Some calcifications made of CA have been detected	1	Papillary thyroid carcinoma stage 2
Patient 5 Biopsy 2	M, 42	Some calcifications made of CA have been detected	1	Papillary thyroid carcinoma stage 2
Patient 5 Biopsy 3	M, 42	Some calcifications made of ACCP have been detected as well as lipids	1	Papillary thyroid carcinoma stage 2
Patient 5 Biopsy 4	M, 42	CA calcifications have been detected	1	Papillary thyroid carcinoma stage 2

CA = carbapatite or calcium phosphate apatite; ACCP = amorphous carbonated calcium phosphate.

2. Experimental

A set of 31 thyroid smears corresponding to 13 patients, coming from the Service de Chirurgie digestive, Générale et Endocrinienne, CHU Dupuytren (Limoges, France) and the Department of Thoracic Surgery of Geneva have been considered (Tables 1 and 2). Of the 13 patients, five (Patient number 1–5) had papillary cancer, two (Patient number 6 and 7) had Graves' disease, six had benign nodules (Nodular goitre Patient number 8–12 and Patient 13 Thyroid adenoma). For one patient (Patient number 9), the thyroid disease was associated with primary hyperparathyroidism (HPT). The smears were ob-

Table 2. Clinical data and chemical compounds identified in smears of thyroid biopsies for patients with Graves' disease, nodular goitre or thyroid adenoma

Samples	Sex and age	FTIR analysis	Bethesda classification	Pathology
Patient 6 Biopsy 1	F, 35	Some calcifications made of CA have been detected	2	Graves' disease
Patient 6 Biopsy 2	F, 35	Some lipids have been detected	2	Graves' disease
Patient 6 Biopsy 3	F, 35	Some calcifications made of CA and lipids have been detected	1	Graves' disease
Patient 7 Biopsy 1	F, 55	No calcification	1	Graves' disease
Patient 8 Biopsy 1	M, 72	Some calcifications made of CA and/or ACCP have been detected	4	Nodular goitre
Patient 8 Biopsy 2	M, 72	Sample without apatite but note the presence of polysaccharides	4	Nodular goitre
Patient 9 Biopsy 1	F, 75	Some calcifications made of CA and/or ACCP have been detected	3	Nodular goitre
Patient 9 Biopsy 2	F, 75	Some calcifications made of CA and/or ACCP have been detected	3	Nodular goitre
P. No 10 Biopsy 1	M, 67	The deposit was too thick	1	Nodular goitre
P. No 10 Biopsy 2	M, 67	The deposit was too thick	1	Nodular goitre
P. No 10 Biopsy 3	M, 67	Some calcifications made of CA and/or ACCP have been detected	1	Nodular goitre
P. No 11 Biopsy 1	F, 31	The deposit was too thick	4	Nodular goitre
P. No 11 Biopsy 2	F, 31	Glycoproteins. No visible calcification	4	Nodular goitre
P. No 12 Biopsy 1	F, 70	Spherical calcifications made of CA and/or ACCP have been detected	1	Nodular goitre
P. No 12 Biopsy 2	F, 70	Spherical calcifications made of CA and/or ACCP have been detected	1	Nodular goitre
P. No 13 Biopsy 1	F, 45	No deposit	2	Thyroid adenoma
P. No 13 Biopsy 2	F, 45	Some calcifications made of CA have been detected	2	Thyroid adenoma

CA = carbapatite; ACCP = amorphous carbonated calcium phosphate.

tained through aspiration, with a fine needle, performed under ultrasound guidance to ensure accurate placement of the needle within the thyroid nodule [32–34]. Calcifications were visualized in 17 of 31 samples taken (55%) (Table 2). Histopathological analysis of the specimens was performed by a senior pathologist. The specimens from patients 1–5 and 11 were re-read by a second pathologist to confirm the

diagnosis.

All patient-derived tissues were collected and archived at the Tumorotheque of Limoges University Hospital, under protocols approved by the Institutional Review Board (AC N 2007-34, DC 2008-604 and 72-201118). Written informed consent was obtained from all subjects of this study. Each sample was only named by a study number, without indication of the name of the patient or potential identification data.

All the calcifications were investigated with a Zeiss SUPRA55-VPFE-SEM in order to describe their morphology at the micrometer scale. To maintain the integrity of the samples, measurements were performed at low voltage (1.0 keV) and without the usual deposits of carbon at the surface of the sample [18,21]. All calcifications were characterized using μFTIR spectrometry (Cary 620 infrared microscope equipped with a 64 × 64 pixels Stingray MCT detector coupled to a Cary 660 spectrometer equipped with a KBr beamsplitter and a Michelson interferometer, LBM, ENS-PSL). Data were collected in the reflexion mode between 4000 and 700 cm^{-1}, with a resolution of 8 cm^{-1}. The different compounds were identified by comparing their IR spectrum to the IR spectrum of reference compounds [35].

3. Results and discussion

3.1. *The point of view of the clinician: the state of the art*

Ultrasonography (US) is the main tool to explore thyroid diseases, especially for detecting nodules, measuring their dimensions, and evaluating any associated changes in the thyroid glands [36]. The use of a standardized US reporting system to analyze US imaging reporting reduces the inconsistency of US descriptive reports and ease the management of thyroid nodules. The most used system is the thyroid imaging reporting and data system (TIRADS) recently updated [37,38]. It has the best correlation with cytologic findings. Suspicious US lesions such as a solid hypoechoic nodule, with a spiculated or lobulated margin or a hypoechoic halo, or the presence of intra nodular calcifications, need fine needle aspiration (FNA). The average malignancy risk of such nodules is around 56% but increases with the number of suspicious features [39–41]. Microcalcifications are a good predictor of malignancy especially in partially cystic nodules [42]. Microcalcifications appear as tiny hyperechoic spots, <1 mm. They correspond to psammomas bodies and are highly suggestive of the most frequent type of thyroid carcinoma, papillary thyroid carcinoma [16,43]. A recent meta-analysis including 41 studies for a total of 29,678 patients demonstrated that microcalcifications were associated with a high risk of malignancy with a 676 odds ratio (OR) [44]. However, if their specificity for malignancy is elevated (85–95%), their sensitivity is low, particularly in nodules under 1 cm diameter [45]. However, the risk of carcinoma does not decrease with nodule size. This risk depends on the ultrasonographic criteria placing the risk at 19.7% vs 7.8% for nodules sized 1 cm or more without suspicious sonographic findings [46].

Such results are in line with a recent investigation performed by Yin *et al.* [47]. These authors found that thyroid microcalcifications and partial macrocalcifications, such as eggshell discontinuous calcifications, and multilayer-like calcifications were associated with thyroid carcinoma (41.4% vs 21%). Eggshell discontinuous macrocalcifications and multilayer-like macrocalcifications also occurred mainly in malignant nodules, while eggshell calcifications in a row are more often seen in benign nodules [47]. The type of calcification is therefore an important predictor of cancer.

The FNA allows to withdraw cells from a suspicious nodule such as a nodule containing microcalcifications or nodule of size >1 cm. FNA under US guidance is recommended because it reduces false-negative cytology, established at around 1% [48]. The three classification systems rank the cytology diagnosis in five major classes and the widely used is the Bethesda System [49] (Table 3).

Classifications depend on cell features. Suspicion of malignancy or malignant results force the patient to be referred to an endocrine surgeon. The risk of malignancy in benign lesion (named Bethesda 2) is about 1% and a clinical or US follow-up is recommended. Two categories are less consistent, Bethesda 3 and Bethesda 1. The first one is the indeterminate category that imposes surgery or careful follow-up because the risk of malignancy is around 15% [50]. The second one is nondiagnostic specimens due to insufficient number of thyroid cells, or virtually acel-

Table 3. The 2017 Bethesda system for reporting thyroid cytopathology, implied risk of malignancy and recommended clinical management [49]

Rank	Diagnostic category	Risk of malignancy	Usual management
Bethesda 1	Non-diagnostic or unsatisfactory	5–10%	Repeat FNA
Bethesda 2	Benign	0–3%	Clinical and sonographic follow-up
Bethesda 3	Atypia or undetermined significance or follicular lesion	10–30%	Repeat FNA or lobectomy
Bethesda 4	Follicular neoplasm or suspicious for a follicular neoplasm	25–40%	Lobectomy
Bethesda 5	Suspicious for malignancy	50–75%	Total thyroidectomy or lobectomy
Bethesda 6	Malignant	97–99%	Total thyroidectomy or lobectomy

lular specimen. In this category, the risk of malignancy is estimated to be 16% [51] and a real evaluation of the need for surgery is necessary. The balance between the risks of a potentially delayed diagnosis of carcinoma that imposes surgery, and those of superfluous surgery should be considered.

In 2015, ATA recommended basing management of thyroid nodules on their risk of malignancy assessed on ultrasound coupled with FNA if the nodules are supra-centimetric. Only Bethesda 2 nodules, i.e. benign, do not require FNA [52]. This risk varies from 10 to 30% for Bethesda 3. Ultrasound, even coupled with cytology, does not therefore make it possible to accurately determine the risk of cancer in a nodule. The development of new methods, like automated machine learning for identifying nodules with high-risk mutations on molecular testing, promises to facilitate the identification of suspicious nodules but is not yet routine practice [53]. The risk is to wrongly operate on benign nodules, and to ignore the cancer in a centimetric or supracentimetric nodule.

3.2. *The point of view of the physico-chemist: more new questions*

In all the above literature dedicated to calcifications present in thyroid, the chemical phases present in the calcifications are not identified through physicochemical techniques. The only parameter which is discussed is the size of the calcifications and two cases are distinguished: micro and macrocalcifications. In an attempt to establish a significant correlation between the pathological calcifications and the pathology, the morphologic characteristics of the pathological calcification as well as their chemical composition must be considered.

For example, whewellite kidney stones, depending on their morphologic features at both macroscopic and mesoscopic scales, can be associated with an alimentation disorder or a genetic abnormality, namely primary hyperoxaluria, each pathology being related to a specific morphology [22,25,54–56]. It is based on the fact that pathologies correspond to very different biochemical conditions leading to the formation of different chemical compounds with different crystallite morphologies [22,24].

Here, we start by a selected presentation of FE-SEM observations. In Figure 1, we have reported the observations performed on the sample B399 (Patient 1, Biopsy 1). We can see micrometer-sized acicular objects. Unfortunately, due to the small thickness of these biological objects we were not able to obtain valuable FTIR spectra.

Other usual morphologies have been obtained on the sample B400 (Patient 1, Biopsy 2, Figure 2). In that case, observation at large magnification (Figure 2C) indicates an agglomeration of crystals. Their morphologies seem to be close to the ones of both weddellite (or COD for calcium oxalate dihydrate) and whewellite (or COM for calcium oxalate monohydrate) [57]. These two crystalline phases of calcium oxalate have been already identified in thyroid calcifications [15,16].

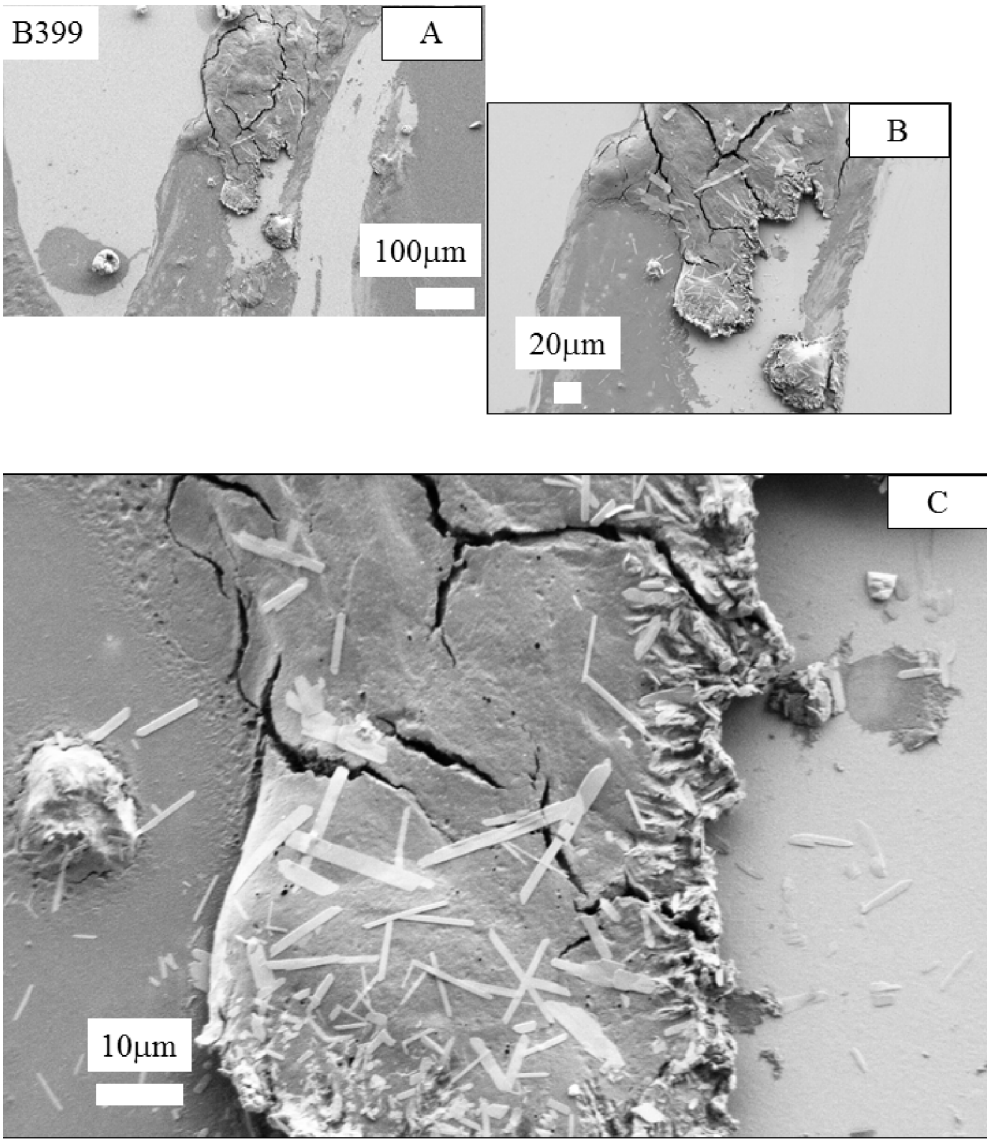

Figure 1. FE-SEM observations at different magnifications obtained for the sample B399. We can note the presence of 10 µm acicular objects which display a very small thickness.

In Figure 3, we have compared this morphology to the ones observed for whewellite (A) and for weddellite (B) in the case of kidney stones to (C,D) weddellite crystals present in thyroid biopsies as shown by Guerlain *et al.* [16].

In Figure 4A (sample B403, Patient 3 Biopsy 2), we have superimposed an optical image as collected by the FTIR spectrometer and a FE-SEM observation at low magnification. Then, we selected an area of interest and increased the magnifications (Figures 4B–D). Figure 4D shows the presence of spherical entities (black arrows), a typical morphology for biological calcium phosphate apatite corresponding to two chemical phases namely either carbonated calcium phosphate apatite (CA) or amorphous carbonated calcium phosphate (ACCP) [59–61]. We have

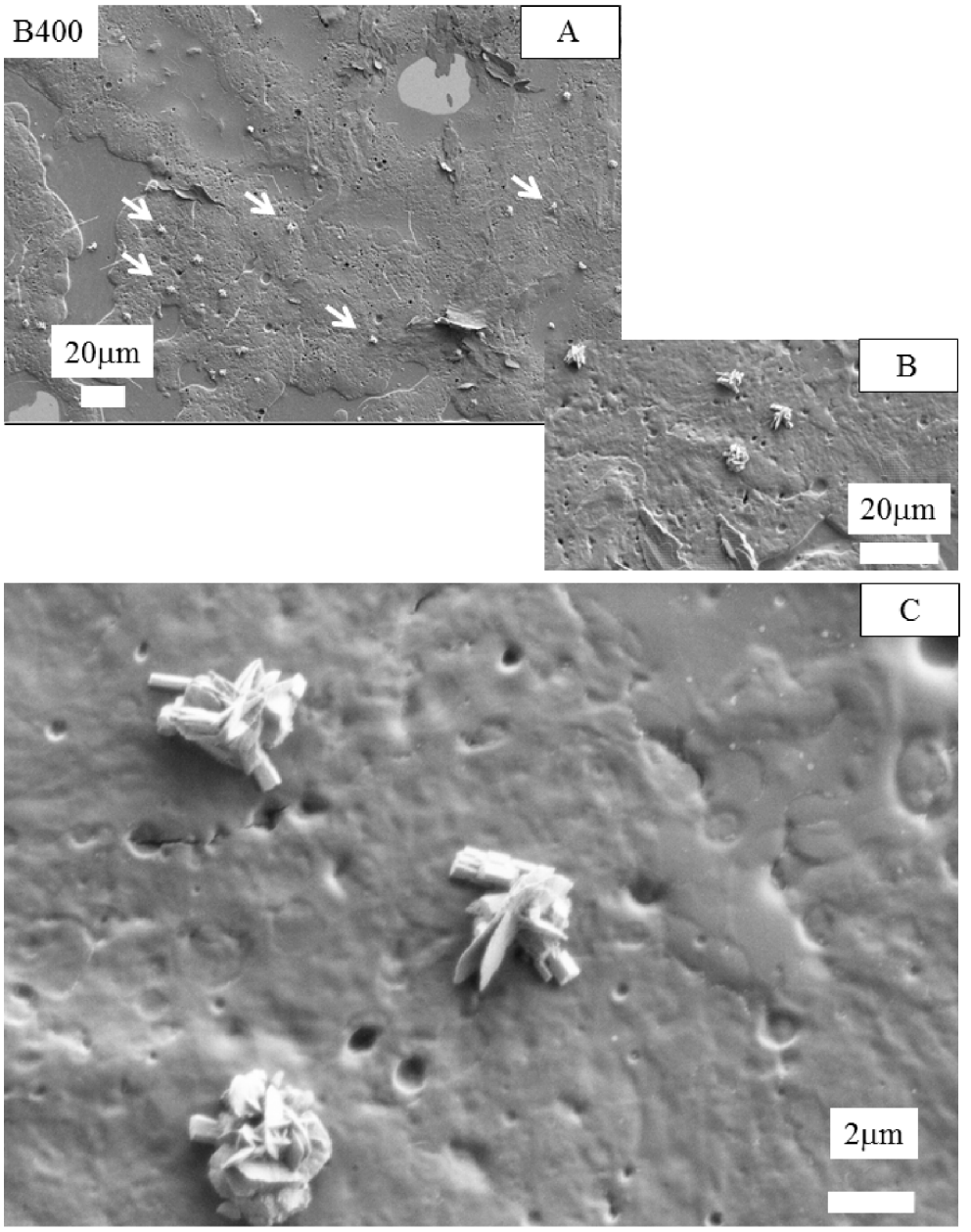

Figure 2. FE-SEM observations at different magnifications obtained for the sample B400 (Patient 1, Biopsy 2). We can note the presence of several aggregates of crystals which have a similar morphology to weddellite and whewellite crystals [57,58].

already found for these two chemical phases such spherical morphology in different parts of the human body, namely kidney [62–68], breast [69–72], skin [73,74], cartilage [75,76] or prostate [77]. At this point, it is worth underlining that spherical entities can be made of calcium carbonate [78]. Note the presence of a crystal (white arrow) probably made of cholesterol.

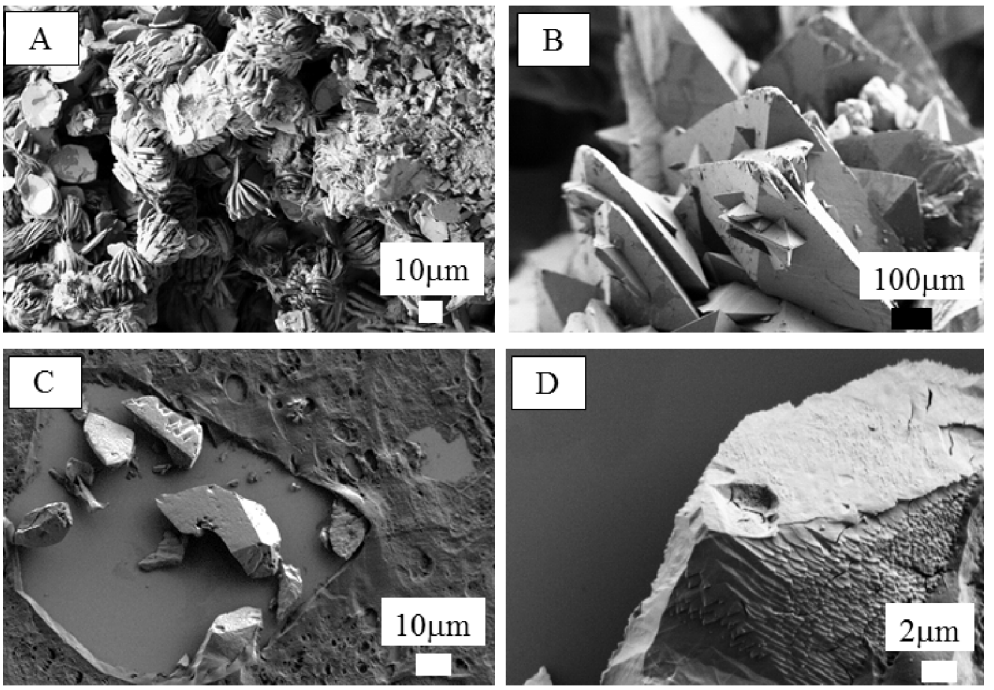

Figure 3. (A) Morphology observed for whewellite (or COM for calcium oxalate monohydrate) and (B) for weddellite (or COD for calcium oxalate dihydrate) in the case of kidney stones. (C,D) Weddellite crystals present in thyroid biopsies as shown by Guerlain *et al.* [16].

In Figure 5A, the optical image present on Figure 4A corresponds to the area where IR spectra have been collected. To build Figure 5B, we have considered the intensity of the IR band at 1000 cm^{-1}, the red part corresponding to high intensity, while the blue one corresponds to low intensity. The B403 (Patient 3 Biopsy 2) sample is shown and compared to FTIR data (Figures 5C and D) which are displayed along with SEM observations (Figure 5D). Significant IR absorption bands underline the presence of ACCP and CA corresponding to the spherical entities (red arrows on Figures 5C and D).

4. Conclusion and perspectives

In this contribution, microcalcifications present in FNA smears of thyroid nodules have been characterized through two different physicochemical techniques namely µFTIR spectroscopy and FE-SEM. Such an approach allows us to obtain their chemical composition as well as morphology at the micrometer scale. The smears were also stained for analysis of the cellular characteristics of these lesions for classifying according to Bethesda classification.

Even if the number of samples is quite low, such an investigation underlines the chemical diversity of the mineral species. Also, FE-SEM observations underline the presence of crystals with unusual morphology which were too small for an accurate identification by µFTIR spectroscopy. We will soon start an investigation using other physicochemical techniques which are able to characterize nanometer scale abnormal deposits, namely a combination of atomic force microscopy and IR spectroscopy [79,80] and optical photothermal IR (OPTIR) spectroscopy [81]. Different publications clearly show that such characterization brings out valuable information in the case of abnormal deposits in biological tissues [72,82–84].

Finally, regarding the relationship between the physico-chemistry of abnormal deposits in thyroid smears and the disease which induces their formation, such a relationship is complex and may depend also on the amount of the compound. In the case of infection, whatever the amount of struvite, this

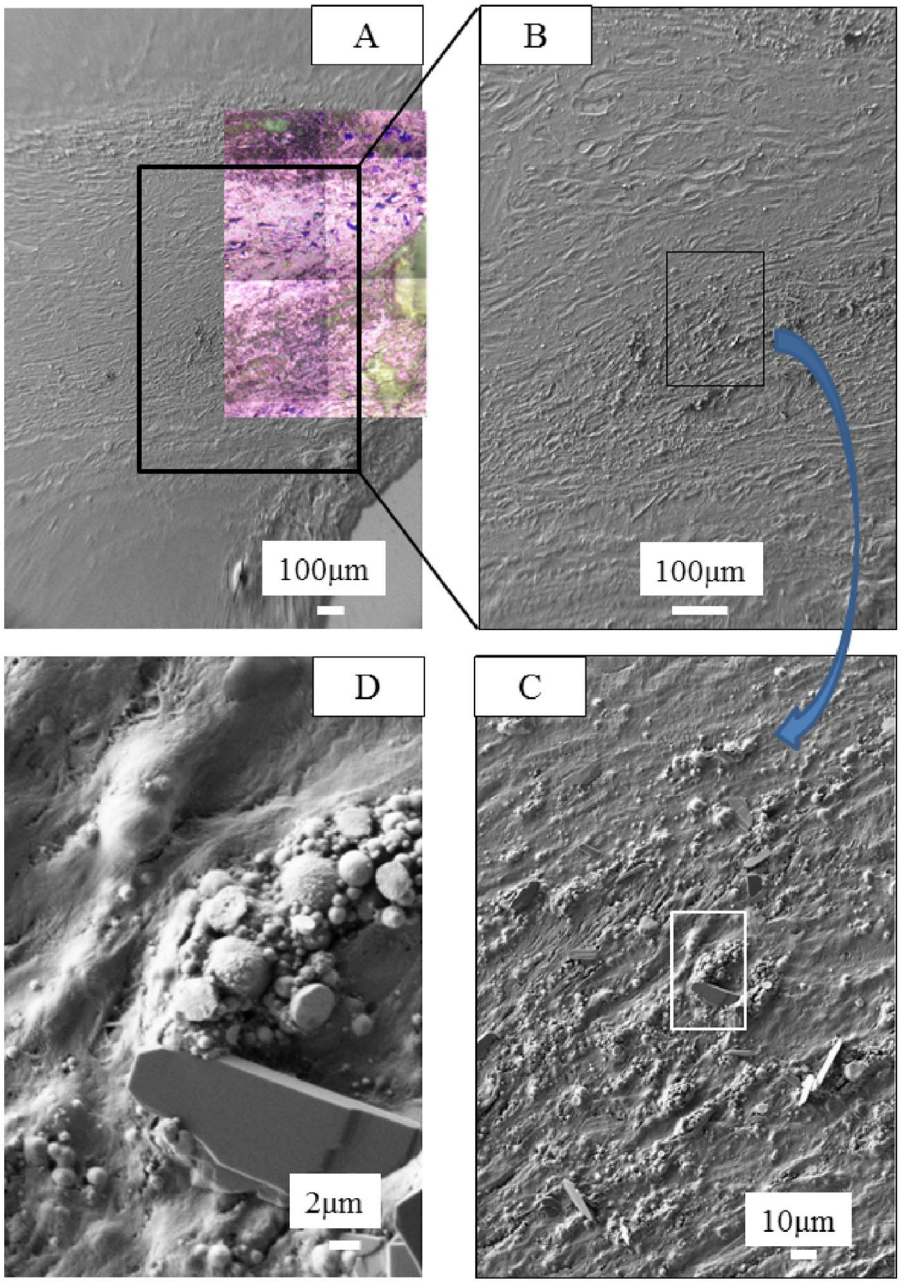

Figure 4. (A) Optical image collected by the FTIR spectrometer with FE-SEM observations at different magnifications (B–D) obtained for the sample B403. Numerous spherical entities (black arrows) are present at the surface and in the smears. Also, a large crystal is also present (white arrow in Figure 4D). Its morphology seems to indicate that it is made of cholesterol.

chemical compound is related to urinary tract infection [85–87]. In the case of whitlockite, its amount in kidney stones has to be greater than 20% (estimated by FTIR) to be related to infection [88,89]. We have thus to define an approach which will be able to identify the different chemical compounds present

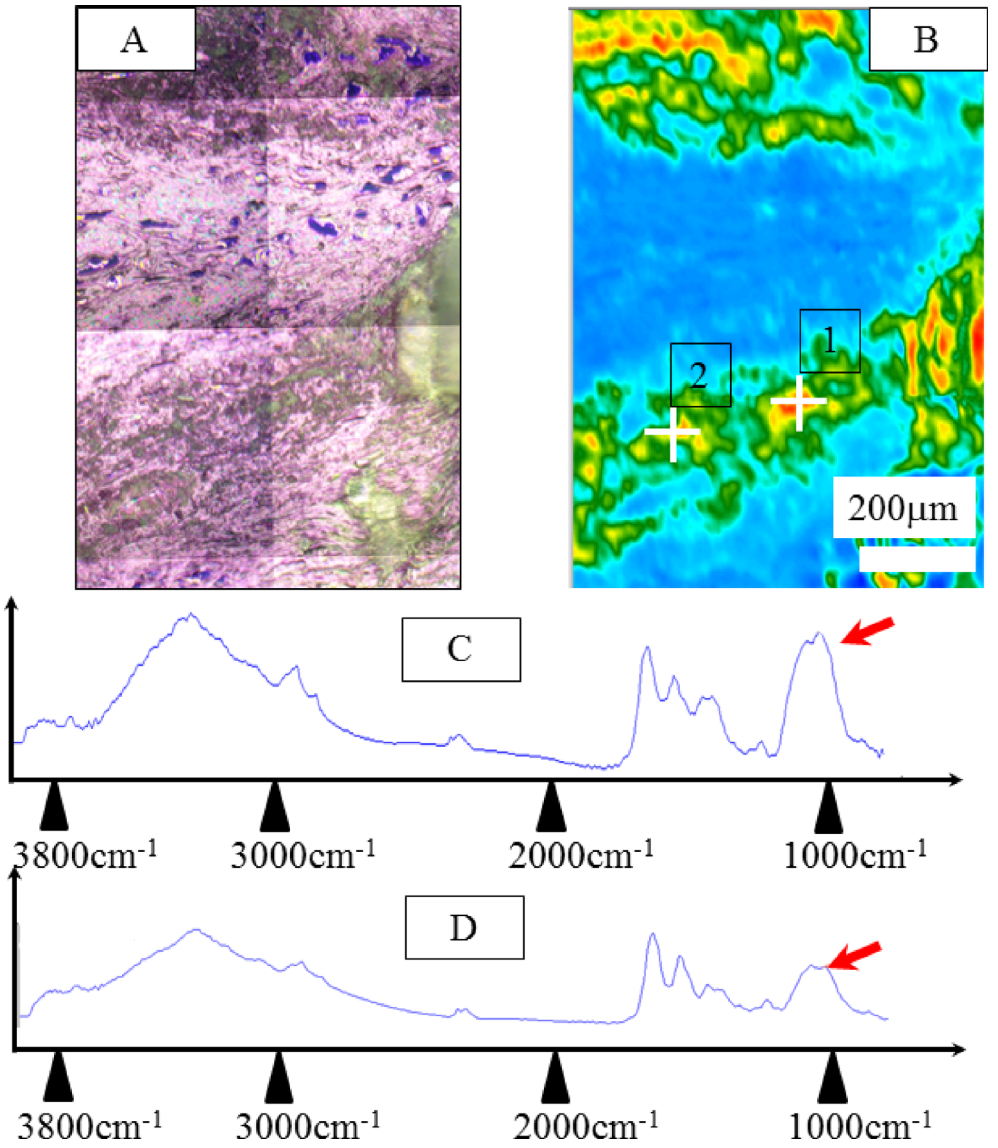

Figure 5. Sample B403. (A) Optical image collected by the FTIR spectrometer (same to Figure 4A). (B) Typical infrared spectrum: ν_3 P-O stretching vibration modes are measured at 1035–1045 cm^{-1}, particular attention has to be paid to the presence of a feature in the ν_3 absorption band, which can be used as a fingerprint for the presence of a mixture of ACCP and CA. (C) and (D) correspond to IR spectra collected respectively to point of interest 1 and 2 of Figure 5B.

in smears, to evaluate their amount and finally to describe the morphology of the abnormal deposits.

Conflicts of interest

Authors have no conflict of interest to declare.

Acknowledgements

We thank ENS-PSL for LH's PhD fellowship, and *Fondation pour la Recherche Biomédicale* (project DEI20151234413) for financial support.

References

[1] A. Maniakas, L. Davies, M. E. Zafereo, *Clin. North Am.*, 2018, **51**, 631-642.

[2] N. Azar, C. Lance, D. Nakamoto, C. Michael, J. Wasman, L. Pantanowitz, *Diagn. Cytopathol.*, 2013, **41**, 1107-1114.

[3] L. Davies, G. Randolph, *Otolaryngol. Clin. North Am.*, 2014, **47**, 461-474.

[4] S. Tamhane, H. Gharib, *Clin. Diabet. Endocrinol.*, 2016, **2**, article no. 17.

[5] J. Luo, C. Zhang, F. Huang, J. Chen, Y. Sun, K. Xu, P. Huang, *Sci. Rep.*, 2017, **7**, article no. 13109.

[6] H. S. Mo, Z. X. Li, S.-D. Wang, X.-H. Liao, M. Liang, X.-Y. Hao, *Int. J. Clin. Exp. Med.*, 2017, **10**, 13473-13481.

[7] R. Wong, S. G. Farrell, M. Grossmann, *Med. J. Aust.*, 2018, **206**, 92-98.

[8] S. Taki, S. Terahata, R. Yamashita, K. Kinuya, K. Nobata, K. Kakuda, Y. Kodama, I. Yamamoto, *Clin. Imag.*, 2004, **28**, 368-371.

[9] J. Jiang, X. Shang, H. Wang, Y.-B. Xu, Y. Gao, Q. Zhou, *Kaohsiung J. Med. Sci.*, 2015, **31**, 138-144.

[10] Q. A. Hassan, A. A. Asghar, M. A. Had, *Int. J. Med. Res. Health Sci.*, 2016, **5**, 148-158.

[11] Y.-J. Tsai, S.-M. Huang, *Ultrasound Med. Biol.*, 2017, **43**, s115-s116.

[12] G. Shandilya, R. K. Sinha, N. Ekka, V. Kumar, *J. Clin. Diagn. Res.*, 2017, **11**, PD01-PD03.

[13] D. Bianchi, U. Morandi, A. Stefani, B. Aramini, *Int. J. Surg. Case Rep.*, 2019, **60**, 46-48.

[14] L. Yin, W. Zhang, W. Bai, W. He, *Ultrasound Med. Biol.*, 2020, **46**, 20-25.

[15] M. Mathonnet, A. Dessombz, D. Bazin, R. Weil, F. Triponez, M. Pusztaszeri, M. Daudon, *C. R. Chim.*, 2016, **19**, 1672-1678.

[16] J. Guerlain, S. Perie, M. Lefevre, J. Perez, S. Vandermeersch, Ch. Jouanneau, L. Huguet, V. Frochot, E. Letavernier, R. Weil, S. Rouzière, D. Bazin, M. Daudon, J.-Ph. Haymann, *PLoS One*, 2019, **14**, article no. e0224138.

[17] D. Bazin, J.-Ph. Haymann, E. Letavernier, J. Rode, M. Daudon, *Presse Med.*, 2014, **43**, 135-148.

[18] D. Bazin, M. Daudon, *Ann. Biol. Clin.*, 2015, **73**, 517-534.

[19] M. Daudon, D. Bazin, *C. R. Chim.*, 2016, **19**, 1416-1423.

[20] D. Bazin, E. Letavernier, J.-P. Haymann, P. Méria, M. Daudon, *Prog. Urol.*, 2016, **26**, 608-618.

[21] D. Bazin, E. Bouderlique, M. Daudon, V. Frochot, J.-Ph. Haymann, E. Letavernier, F. Tielens, R. Weil, *C. R. Chim.*, 2022, **25**, no. S1, 37-60.

[22] M. Daudon, C. A. Bader, P. Jungers, *Scan. Microsc.*, 1993, **7**, 1081-1104.

[23] M. Daudon, P. Jungers, D. Bazin, *AIP Conf. Proc.*, 2008, **1049**, 199-215.

[24] M. Daudon, A. Dessombz, V. Frochot, E. Letavernier, J. P. Haymann, P. Jungers, D. Bazin, *C. R. Chim.*, 2016, **19**, 1470-1491.

[25] M. Daudon, P. Jungers, D. Bazin, *New Engl. J. Med.*, 2008, **359**, 100-102.

[26] D. Bazin, M. Daudon, C. Combes, C. Rey, *Chem. Rev.*, 2012, **112**, 5092-5120.

[27] D. Bazin, M. Daudon, *J. Phys. D: Appl. Phys.*, 2012, **45**, article no. 383001.

[28] A. Dessombz, E. Letavernier, J.-Ph. Haymann, D. Bazin, M. Daudon, *J. Urol.*, 2015, **193**, 1564-1569.

[29] D. Bazin, Ch. Jouanneau, S. Bertazzo, Ch. Sandt, A. Dessombz, M. Réfrégiers, P. Dumas, J. Frederick, J.-Ph. Haymann, E. Letavernier, P. Ronco, M. Daudon, *C. R. Chim.*, 2016, **19**, 1439-1454.

[30] E. Tsolaki, S. Bertazzo, *Materials*, 2019, **12**, article no. 3126.

[31] D. Bazin, E. Letavernier, J. P. Haymann, V. Frochot, M. Daudon, *Ann. Biol. Clin.*, 2020, **78**, 349-362.

[32] P. D. Gutman, M. Henry, *Clin. Lab. Med.*, 1998, **18**, 461-482.

[33] N. Hayashi, M. Kitaoka, *Nihon Rinsho.*, 2007, **65**, 2003-2007.

[34] E. M. Khan, R. Pandey, *Acta Cytol.*, 1996, **40**, 959-962.

[35] N. Quy Dao, M. Daudon, *Infrared and Raman Spectra of Calculi*, Elsevier, Paris, 1997.

[36] L. Solbiati, V. Osti, L. Cova, M. Tonolini, *Eur. Radiol.*, 2001, **11**, 2411-2424.

[37] P. Trimboli, R. Ngu, B. Royer, L. Giovanella, C. Bigorgne, R. Simo, P. Caroll, G. Russ, *Clin. Endocrinol.*, 2019, **91**, 340-347.

[38] F. N. Tessler, W. D. Middleton, E. G. Grant, J. K. Hoang, L. L. Berland, S. A. Teefey, J. J. Cronan, M. D. Beland, T. S. Desser, M. C. Frates, L. W. Hammers, U. M. Hamper, J. E. Langer, C. C. Reading, L. M. Scoutt, A. T. Stavros, *J. Am. Coll. Radiol.*, 2017, **14**, 587-595.

[39] G. Russ, B. Royer, C. Bigorgne, A. Rouxel, M. Bienvenu-Perrard, L. Leenhardt, *Eur. J. Endocrinol.*, 2013, **15**, 649-655.

[40] P. Seifert, R. Görges, M. Zimny, M. C. Kreissl, S. Schenke, *Endocrine*, 2020, **67**, 143-155.

[41] G. Russ, S. J. Bonnema, M. F. Erdogan, C. Durante, R. Ngu, L. Leenhardt, *Eur. Thyroid*, 2017, **6**, 225-237.

[42] D. G. Na, D. S. Kim, S. J. Kim, J. W. Ryoo, S. L. Jung, *Ultrasonography*, 2016, **35**, 212-219.

[43] Y. J. Hong, E. J. Son, E. K. Kim, J. Y. Kwak, S. W. Hong, H. S. Chang, *Clin. Imag.*, 2010, **34**, 127-133.

[44] F. Ianni, P. Campanella, C. A. Rota, A. Prete, L. Castellino, A. Pontecorvi, S. M. Corsello, *Endocrine*, 2016, **51**, 313-321.

[45] M. C. Chammas, V. J. de Araujo Filho, R. A. Moysés, M. D. Brescia, G. C. Mulatti, L. G. Brandao, G. G. Cerri, A. R. Ferraz, *Head Neck*, 2008, **30**, 1206-1210.

[46] Y. H. Bo, H. Y. Ahn, Y. H. Lee, Y. J. Lee, J. H. Kim, J. H. Ohn, E. S. Hong, K. W. Kim, I. K. Jeong, S. H. Choi, S. Lim, D. J. Park, H. C. Jang, B. H. Oh, B. Y. Cho, Y. J. Park, *J. Korean Med. Sci.*, 2011, **26**, 237-242.

[47] L. Yin, W. Zhang, W. Bai, W. He, *Ultrasound Med. Biol.*, 2020, **46**, 20-25.

[48] H. Gharib, E. Papini, J. R. Garber, D. S. Duicks, R. M. Harrell, L. Hegedüs, R. Paschke, R. Valcavi, P. Vitti, *Endocr. Pract.*, 2016, **22**, 622-639.

[49] E. S. Cibas, S. Z. Ali, *Thyroid*, 2017, **27**, 1341-1346.

[50] P. A. Vanderlaan, J. F. Krane, E. S. Cibas, *Acta Cytol.*, 2011, **55**, 512-517.

[51] M. Bongiovanni, C. Bellevicine, G. Troncone, G. P. Sykiotis, *Gland Surg.*, 2019, **8**, S98-S104.

[52] B. R. Haugen, E. K. Alexander, G. M. Doherty, S. J. Mandel, Y. E. Nikiforov, F. Pacini, G. W. Randolph, A. M. Sawka, M. Schlumberger, K. G. Schuff, S. I. Sherman, J. A. Sosa, D. L. Steward, R. M. Tuttle, L. Wartofsky, *Thyroid*, 2016, **26**, 1-133.

[53] K. Daniels, S. Gummadi, Z. Zhu, S. Wang, J. Patel, B. Swendseid, A. Lyshchik, J. Curry, E. Cottrill, J. Eisenbrey, *JAMA Otolaryngol. Head Neck Surg.*, 2020, **146**, 36-41.

[54] M. Daudon, D. Bazin, G. André, P. Jungers, A. Cousson, P. Chevallier, E. Véron, G. Matzen, *J. Appl. Cryst.*, 2009, **42**, 109-115.

[55] D. Bazin, C. Leroy, F. Tielens, Ch. Bonhomme, L. Bonhomme-Coury, F. Damay, D. Le Denmat, J. Sadoine, J. Rode, V. Frochot, E. Letavernier, J. Ph. Haymann, M. Daudon, *C. R. Chim.*, 2016, **19**, 1492-1503.

[56] F. Meiouet, S. El Kabbaj, J. M. Daudon, *C. R. Chim.*, 2022, **25**, no. S1, 281-293.

[57] I. Petit, G. D. Belletti, T. Debroise, M. J. Llansola-Portoles, I. T. Lucas, C. Leroy, Ch. Bonhomme, L. Bonhomme-Coury, D. Bazin, M. Daudon, E. Letavernier, J. Ph. Haymann, V. Frochot, F. Babonneau, P. Quaino, F. Tielens, *Chem. Select*, 2018, **3**, 8801-8812.

[58] X. Sheng, M. D. Ward, J. A. Wesson, *J. Am. Soc. Nephrol.*, 2005, **16**, 1904-1908.

[59] C. Rey, C. Combes, C. Drouet, A. Lebugle, H. Sfihi, A. Barroug, *Mater. Sci. Eng. Technol. C*, 2007, **38**, 996-1002.

[60] C. Rey, C. Combes, C. Drouet, H. Sfihi, A. Barroug, *Mater. Sci. Eng.: C*, 2007, **27**, 198-205.

[61] C. Drouet, C. Rey, "Nanostructured calcium phosphates for hard tissue engineering and nanomedicine", in *Nanostructured Biomaterials for Regenerative Medicine* (V. Guarino, M. Iafisco, S. Spriano, eds.), Woodhead Publishing Series in Biomaterials, Woodhead Publishing, Sawston, UK, 2020, 223-254.

[62] D. Bazin, V. Frochot, J.-Ph. Haymann, E. Letavernier, M. Daudon, *C. R. Chim.*, 2022, **25**, no. S1, 133-147.

[63] N. Çiftçioğlu, K. Vejdani, O. Lee, G. Mathew, K. M. Aho, E. O. Kajander, D. S. McKay, J. A. Jones, M. L. Stoller, *Int. J. Nanomed.*, 2008, **3**, 105-115.

[64] X. Carpentier, M. Daudon, O. Traxer, P. Jungers, A. Mazouyes, G. Matzen, E. Véron, D. Bazin, *Urology*, 2009, **73**, 968-975.

[65] S. R. Khan, B. K. Canales, *Urolithiasis*, 2015, **43**, 109-123.

[66] C. Verrier, D. Bazin, L. Huguet, O. Stéphan, A. Gloter, M.-Ch. Verpont, V. Frochot, J.-Ph. Haymann, I. Brocheriou, O. Traxer, M. Daudon, E. Letavernier, *J. Urol.*, 2016, **196**, 1566-1574.

[67] E. Letavernier, G. Kauffenstein, L. Huguet, N. Navasiolava, E. Bouderlique, E. Tang, L. Delaitre, D. Bazin, M. de Frutos, C. Gay, J. Perez, M. C. Verpont, J.-Ph. Haymann, V. Pomozi, J. Zoll, O. Le Saux, M. Daudon, G. Leftheriotis, L. Martin, *J. Am. Soc. Nephrol.*, 2018, **29**, 2337-2347.

[68] C. Gay, E. Letavernier, M.-Ch. Verpont, M. Walls, D. Bazin, M. Daudon, N. Nassif, O. Stephan, M. de Fruto, *ACS Nano*, 2020, **14**, 1823-1836.

[69] A. Ben Lakhdar, M. Daudon, M.-Ch. Mathieu, A. Kellum, C. Balleyguier, D. Bazin, *C. R. Chim.*, 2016, **19**, 1610-1624.

[70] J. A. M. R. Kunitake, S. Choi, K. X. Nguyen, M. M. Lee, F. He, D. Sudilovsky, P. G. Morris, M. S. Jochelson, C. A. Hudis, D. A. Muller, P. Fratzl, C. Fischbach, A. Masi, L. A. Estroff, *J. Struct. Biol.*, 2018, **202**, 25-34.

[71] K. S. Shin, M. Laohajaratsang, S. Men, B. Figueroa, S. M. Dintzis, D. Fu, *Theranostics*, 2020, **10**, 5865-5878.

[72] M. Petay, M. Cherfan, E. Bouderlique, S. Reguer, J. Mathurin, A. Dazzi, M. l'Heron, M. Daudon, V. Frochot, J.-Ph. Haymann, E. Letavernier, A. Deniset-Besseau, D. Bazin, *C. R. Chim.*, 2022, **25**, no. S1, 553-576.

[73] H. Colboc, J. Fontaine, D. Bazin, V. Frochot, E. Letavernier, M. Daudon, N. Laporte, S. Rouzière, M. Reby, A. Galezowski, Ch. Forasassi, S. Meaume, *J. Gerontol. A: Biol. Sci. Med. Sci.*, 2022, **77**, 27-32.

[74] H. Colboc, Ph. Moguelet, E. Letavernier, V. Frochot, J.-F. Bernaudin, R. Weil, S. Rouzière, P. Seneth, C. Bachmeyeri, N. Laporte, I. Lucas, V. Descamps, R. Amodek, F. Brunet-Possentik, N. Kluger, L. Deschamps, A. Dubois, S. Reguer, A. Somogyi, K. Medjoubi, M. Refregiers, M. Daudon, D. Bazin, *C. R. Chim.*, 2022, **25**, no. S1, 445-476.

[75] Ch. Nguyen, D. Bazin, M. Daudon, A. Chatron-Colliet, D. Hannouche, A. Bianchi, D. Côme, A. So, N. Busso, F. Lioté, H.-K. Ea, *Arthritis Res. Therapy*, 2013, **15**, article no. R103.

[76] A. Gauffenic, D. Bazin, Ch. Combes, M. Daudon, H.-K. Ea, *C. R. Chim.*, 2022, **25**, no. S1, 517-534.

[77] A. Dessombz, P. Méria, D. Bazin, M. Daudon, *PLoS One*, 2021, **7**, article no. e5169.

[78] H. Colboc, D. Bazin, Ph. Moguelet, V. Frochot, R. Weil, E. Letavernier, Ch. Jouanneau, C. Frances, C. Bachmeyer, J.-F. Bernaudin, M. Daudon, *C. R. Chim.*, 2016, **19**, 1631-1641.

[79] A. Dazzi, C. B. Prater, *Chem. Rev.*, 2017, **17**, 5146-5173.

[80] J. Mathurin, A. Deniset-Besseau, D. Bazin, E. Dartois, M. Wagner, A. Dazzi, *J. Appl. Phys.*, 2022, **131**, article no. 010901.

[81] D. Fournier, F. Lepoutre, A. Boccara, *J. Phys.*, 1983, **44**, 479-482.

[82] E. Esteve, Y. Luque, J. Waeytens, D. Bazin, L. Mesnard, Ch. Jouanneau, P. Ronco, A. Dazzi, M. Daudon, A. Deniset-Besseau, *Anal. Chem.*, 2020, **92**, 7388-7392.

[83] D. Bazin, M. Rabant, J. Mathurin, M. Petay, A. Deniset-Besseau, A. Dazzi, Y. Su, E. P. Hessou, F. Tielens, F. Borondics, M. Livrozet, E. Bouderlique, J.-Ph. Haymann, E. Letavernier, V. Frochot, M. Daudon, *C. R. Chim.*, 2022, **25**, no. S1, 489-502.

[84] D. Bazin, E. Bouderlique, E. Tang, M. Daudon, J.-Ph. Haymann, V. Frochot, E. Letavernier, E. Van de Perre, J. C. Williams, Jr., J. E. Lingeman, F. Borondics, *C. R. Chim.*, 2022, **25**, no. S1, 105-131.

[85] X. Carpentier, M. Daudon, O. Traxer, P. Jungers, A. Mazouyes, G. Matzen, E. Véron, D. Bazin, *Urology*, 2009, **73**, 968-975.

[86] D. Bazin, G. André, R. Weil, G. Matzen, E. Véron, X. Carpentier, M. Daudon, *Urology*, 2012, **79**, 786-790.

[87] M. Daudon, M. Petay, S. Vimont, A. Deniset, F. Tielens, J.-Ph. Haymann, E. Letavernier, V. Frochot, D. Bazin, *C. R. Chim.*, 2022, **25**, no. S1, 315-334.

[88] L. Maurice-Estepa, P. Levillain, B. Lacour, M. Daudon, *Scand. J. Urol. Nephrol.*, 1999, **33**, 299-305.

[89] D. Bazin, R. J. Papoular, E. Elkaim, R. Weil, D. Thiaudière, C. Pisapia, B. Ménez, N. S. Hwang, F. Tielens, M. Livrozet, E. Bouderlique, J.-P. Haymann, E. Letavernier, L. Hennet, V. Frochot, M. Daudon, *C. R. Chim.*, 2022, **25**, no. S1, 343-354.